

AD A 030727

AFGL-TR-76-0116
ENVIRONMENTAL RESEARCH PAPERS, NO. 562



Plasma Heating Through Parametrically Induced Turbulence

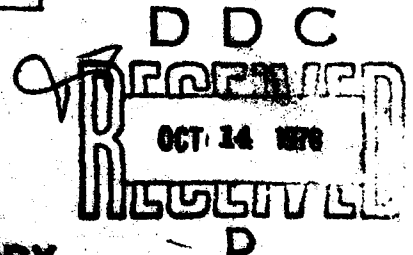
ARTHUR L PAVEL, Capt, USAF

2 June 1976

Approved for public release; distribution unlimited.

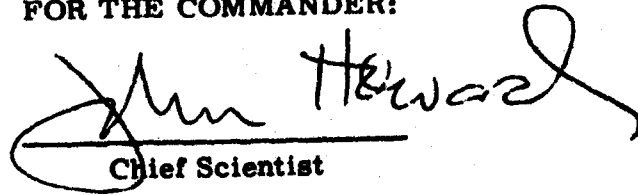
SPACE PHYSICS DIVISION PROJECT 8600
AIR FORCE GEOPHYSICS LABORATORY
HANSCOM AFB, MASSACHUSETTS 01731

AIR FORCE SYSTEMS COMMAND, USAF



This technical report has been reviewed and
is approved for publication.

FOR THE COMMANDER:


Chief Scientist

Qualified requestors may obtain additional copies from the Defense
Documentation Center. All others should apply to the National
Technical Information Service.

Unclassified

SECURITY CLASSIFICATION OF THIS PAGE (When Data Entered)

REPORT DOCUMENTATION PAGE		READ INSTRUCTIONS BEFORE COMPLETING FORM	
1. REPORT NUMBER AFGL-TR-76-116, AFGL-ERP-562	2. GOVT ACCESSION NO.	3. RECIPIENT'S CATALOG NUMBER	
4. TITLE AND SUBTITLE PLASMA HEATING THROUGH PARAMETRICALLY INDUCED TURBULENCE.		5. TYPE OF REPORT & PERIOD COVERED Scientific. Interim.	
7. AUTHOR(s) Arthur L. Pavel / Capt, USAF		6. PERFORMING ORG. REPORT NUMBER ERP No. 562	
9. PERFORMING ORGANIZATION NAME AND ADDRESS Air Force Geophysics Laboratory (PHE) Hanscom AFB Massachusetts 01731		8. CONTRACT OR GRANT NUMBER(s)	
11. CONTROLLING OFFICE NAME AND ADDRESS Air Force Geophysics Laboratory (PHE) Hanscom AFB Massachusetts 01731		10. PROGRAM ELEMENT, PROJECT, TASK AREA & WORK UNIT NUMBERS 61102F 86909D2	16. AF-8692
14. MONITORING AGENCY NAME & ADDRESS (if different from Controlling Office)		12. REPORT DATE 2 June 1976	
		13. NUMBER OF PAGES 27	
		15. SECURITY CLASS. (of this report) Unclassified	
		15a. DECLASSIFICATION/DOWNGRADING SCHEDULE	
16. DISTRIBUTION STATEMENT (of this Report) Approved for public release; distribution unlimited.			
17. Environmental research papers.			
18. SUPPLEMENTARY NOTES			
19. KEY WORDS (Continue on reverse side if necessary and identify by block number) Plasma Plasma instabilities Parametric instabilities Plasma heating			
20. ABSTRACT (Continue on reverse side if necessary and identify by block number) Electromagnetic waves have been shown to be capable of significantly modifying both the magnetospheric and ionospheric plasma. Laboratory studies of the plasma instabilities generated in microwave-plasma interactions have helped to understand the geophysical experiments. Microwave-plasma research has also been useful in modeling the interaction of lasers and plasmas, particularly in relation to efforts using pulsed lasers to compress and heat plasma to thermonuclear conditions.			

DD FORM 1473 EDITION OF 1 NOV 65 IS OBSOLETE

Unclassified

SECURITY CLASSIFICATION OF THIS PAGE (When Data Entered)

409578

X

Unclassified

SECURITY CLASSIFICATION OF THIS PAGE(When Data Entered)

An experiment is described which investigates the evolution of the parametric instability which occurs with near resonant matching of the microwave frequency and plasma frequency. Near threshold, a finely detailed spectrum of satellite electron plasma waves is observed. These waves break down into a turbulent plasma condition with a marked change in power absorbed by the plasma. The plasma passes through several distinctive regimes of turbulent plasma conditions. At the highest power levels used, there are plasma waves hundreds of megacycles from the driving frequency. The plasma is found to absorb a significant amount of power and heat electrons to high energies.



Unclassified

SECURITY CLASSIFICATION OF THIS PAGE(When Data Entered)

ACCESSION for	
DTIS	White Section <input checked="" type="checkbox"/>
DDC	Buff Section <input type="checkbox"/>
UNANNOUNCED	<input type="checkbox"/>
JUSTIFICATION	
BY	
DISTRIBUTION AVAILABILITY CODES	
Dist. / Availability of SPECIAL	
A	

Contents

1. INTRODUCTION	5
1.1 The Parametric Instability	6
1.2 Interaction Model	7
2. EXPERIMENTAL APPARATUS	9
2.1 Plasma Characteristics	11
2.2 Electromagnetic Wave Source and System	13
3. EXPERIMENTAL OBSERVATIONS	14
3.1 Threshold Conditions	14
3.2 Breakdown of Satellite Structure	17
3.3 Plasma Wave Spreading to High Frequencies	19
3.4 Plasma Electron Heating	21
3.5 Ion Acoustic Turbulence	24
4. SUMMARY	25
REFERENCES	27

Illustrations

1. Electromagnetic wave oscillates electrons about their positions in the ion acoustic wave.	6
2. Waveguide walls removed and replaced with high transparency conducting mesh.	10

DDC
 RECEIVED
 OCT 14 1976
 RECEIVED
 D

Illustrations

3. Vacuum chamber with penetrating waveguide.	11
4. Plasma surrounding the filaments.	12
5. Plasma balance is maintained because loss rate is determined by the density.	12
6. Experimental apparatus which allows well-defined electromagnetic wave propagating in a waveguide to interact with large surrounding plasma.	14
7. Threshold plasma wave spectra.	16
8. Plasma wave structure transition to turbulent conditions.	18
9. Computer simulation studies of electron plasma waves driven with a small frequency separation.	19
10. Turbulent plasma wave spectra.	20
11. Electron plasma waves have exponential decay towards higher frequencies.	21
12. Change in structure of absorbed power curve commensurate with breakdown from finely structured electron plasma waves to more turbulent plasma conditions.	22
13. Electron energy distribution retains a Maxwellian energy distribution for moderate power levels.	23
14. For higher power levels the electron energy distribution splits into two segments.	24
15. Ion acoustic turbulence increases to high levels and then appears to saturate at that level.	25

Plasma Heating Through Parametrically Induced Turbulence

1. INTRODUCTION

Electromagnetic waves have been shown to be capable of significantly modifying both the magnetospheric and ionospheric plasma.^{1,2} Laboratory studies of the plasma instabilities generated in microwave-plasma interactions have helped to understand the geophysical experiments. Microwave-plasma research has also been found useful in modeling the interaction of lasers and plasma, particularly in relation to efforts using pulsed lasers to compress and heat plasma to thermonuclear conditions.^{3,4}

An experiment is described which investigates the evolution of the parametric instability which occurs with near resonant matching of the microwave frequency and plasma frequency. Near threshold, a finely detailed spectrum of satellite electron plasma waves is observed. These waves break down into a turbulent plasma condition with a marked change in power absorbed by the plasma.

(Received for publication 28 May 1976)

1. Cohen, R. and Whitehead, J.D. (1970) J. Geophys. Res. 75:6439.
2. Carlson, H.E., Gordon, W.E. and Showen, R.L. (1972) J. Geophys. Res. 77:1242-1250.
3. Chu, T.K. and Hendel, H.W. (1972) Phys. Rev. Lett. 29:634.
4. Dreiser, H., Ellis, R.F. and Ingraham, T.C. (1973) Phys. Rev. Lett. 31:426.

The plasma passes through several distinctive regimes of turbulent plasma conditions. At the highest power levels used, there are plasma waves hundreds of megacycles from the driving frequency. The plasma is found to absorb a significant amount of power and heat electrons to high energies.

1.1 The Parametric Instability

A plasma exhibits many characteristic modes of oscillation of the plasma particles. In a magnetic-free plasma these modes are electron-plasma, or Langmuir, oscillations, which are the reaction of the plasma electrons to a density perturbation and the resulting oscillation at the Bohm-Gross frequency, and ion acoustic oscillations, where the electron pressure provides a force which allows a charge imbalance at a lower frequency.

The application of a high-frequency electromagnetic wave to a plasma will initially be felt only by the plasma electrons, since the much more massive ions will be unable to react.

There are ion acoustic waves present in all plasmas; these waves arise from the statistical charge density fluctuations which occur naturally in a plasma. The waves are continually being created, damping away, and being recreated. Because of the charge neutrality of a plasma and the much greater mobility of the electrons than the ions, the electron density will parallel the ion density closely.

The electromagnetic wave will then oscillate the electrons at a high frequency about their positions in the ion acoustic wave, as shown in Figure 1. Through this mechanism, an electromagnetic wave couples with an ion fluctuation and produces an electron plasma wave.

If certain frequency matching conditions are satisfied, the electromagnetic wave will interact with the electric field of the oscillating electron plasma wave to form a "beat" frequency at or around the ion acoustic frequency. This "beat" frequency will exert a force at a sufficiently low frequency that the ions will be influenced by it. The existing ion density fluctuations will be amplified. As the ion fluctuations grow, charge neutrality demands that the electron fluctuations grow with them.

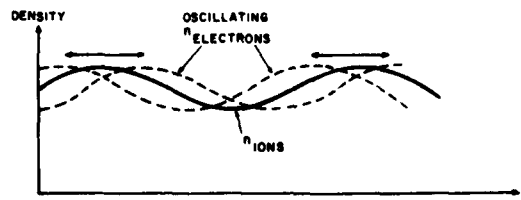


Figure 1. Electromagnetic wave oscillates electrons about their positions in the ion acoustic wave

An experimental investigation of this effect is the topic of this report.

1.2 Interaction Model

When the displacement of the electrons is small compared to the wavelength of the ion acoustic wave, certain approximations can be made and a simplified description of the electromagnetic wave and plasma wave interaction is possible. The more massive ions will not respond directly to the electromagnetic wave, while the electrons do respond and oscillate at the electromagnetic wave frequency. From this situation two frames of reference are created: one with the still ions (x) and one with the driven electrons (x').

Let the ion density be (where the \sim 's represent the relatively small plasma wave terms):

$$n_i = n + \tilde{n}_i(t) e^{i kx}$$

and the electron density be:

$$n_e = n + \tilde{n}_e(t) e^{i kx'}$$

The electrons are being oscillated by the high-frequency electromagnetic field:

$$E = E_0 \sin \omega_0 t.$$

The electromagnetic wavelength is neglected because it is very long compared to the longitudinal plasma wavelengths. This results in the electron frame of reference moving with respect to the x coordinate:

$$x' = x - (eE_0 / m\omega_0^2) \sin \omega_0 t.$$

The maximum displacement of the electrons will be:

$$d = eE_0 / m\omega_0^2$$

The one-dimensional plasma hydrodynamic equations (with $T_e \gg T_i$), an equation of state, and Poisson's equation can now be applied to this situation.

Second order effects are neglected, and the equations are combined to yield an analytical description of the plasma density fluctuations under the influence of an electromagnetic wave. If the displacement of the electrons is small compared to the wavelength ($Rd \ll 1$), the following approximations can be made:

$$e^{\pm ik(x' - x)} \approx 1 \mp ik \left(\frac{eE_0}{m \omega_0^2} \right) \sin \omega_0 t.$$

The resulting coupled non-linear equations are:
for the ion fluctuations:

$$\left(\frac{\partial^2 \tilde{n}_i}{\partial t^2} \right) + \omega_i^2 \tilde{n}_i = - \left(\frac{ikeE_0}{mi} \right) \left(\frac{\omega_{pe}^2}{\omega_0^2} \right) \tilde{n}_e \sin \omega_0 t$$

for the electron fluctuations:

$$\left(\frac{\partial^2 \tilde{n}_e}{\partial t^2} \right) + \omega_e^2 \tilde{n}_e = \left(\frac{ikeE_0}{m_e} \right) \left(\frac{\omega_{pe}^2}{\omega_0^2} \right) \tilde{n}_i \sin \omega_0 t.$$

In these two equations are the two natural modes of oscillation of a plasma, which reflects the harmonic oscillatory motion of a plasma at the ion acoustic frequency, ω_i , and at the Bohm-Gross frequency, ω_e . But, also in these equations, it is clear that the two modes of oscillation are coupled together by the electromagnetic wave.

Matching conditions and growth rates for the instability can be analyzed by expanding the ion and electron densities into slowly and rapidly varying components:

$$\tilde{n}_i = C_i(t) e^{i\omega_i t} + C_i^*(t) e^{-i\omega_i t}$$

$$\tilde{n}_e = C_e(t) e^{i\omega_e t} + C_e^*(t) e^{-i\omega_e t}.$$

Relative to the ω 's, the C 's are slowly varying functions of time. Expanding the harmonic equations, and then time averaging over the fast time scale, reveals that growth of the density fluctuations is only possible when certain frequency conditions are satisfied. One such condition is:

$$\omega_0 = \omega_e + \omega_i$$

This particular condition is important because $\omega_0 > \omega_{pe}$ and the electromagnetic wave can penetrate the plasma.

When the resonance matching conditions are satisfied, a time average over the plasma equations can remove the high-frequency components of these equations. Only the relatively slowly varying C's will remain in the equations:

$$\ddot{C}_i + 2\omega_i \dot{C}_i = -\frac{1}{2} \omega_{pi}^2 k d C_e$$

$$\ddot{C}_e + 2\omega_e \dot{C}_e = -\frac{1}{2} \omega_{pe}^2 k d C_i$$

Since the requirements of plasma neutrality demand that the low-frequency density fluctuations remain equal, with the much more mobile electrons following the ion fluctuations, the ion and electron fluctuations will grow together. The following approximation can, therefore, be made:

$$C_e = C_i = C_e \delta t$$

Substitution of this result into the plasma equations yields for the growth rate, δ :

$$|\delta| = \left| \frac{\omega_{pe}^2 k d (m_e/m_i)^{\frac{1}{2}}}{4 (\omega_i \omega_e)^{\frac{1}{2}}} \right|$$

Phenomena which act to damp away the plasma wave modes that arise always exist. In order for any particular mode to have significant growth, it first must be excited strongly enough to overcome this damping. This level of excitation is the threshold for the instability. The normal damping mechanisms are collisions acting on the electrons and Landau damping of the ions.

2. EXPERIMENTAL APPARATUS

For this experiment a device was constructed which allows a large, uniform, collisionless, magnetic field free, Maxwellian plasma to interact, in a controlled situation, with a well-defined electromagnetic wave propagating in a waveguide.

The fundamental concept behind the device was to remove the walls of the waveguide in the direction of the electric field and replace them with a high transparency conducting mesh. This mesh would contain the E & M wave

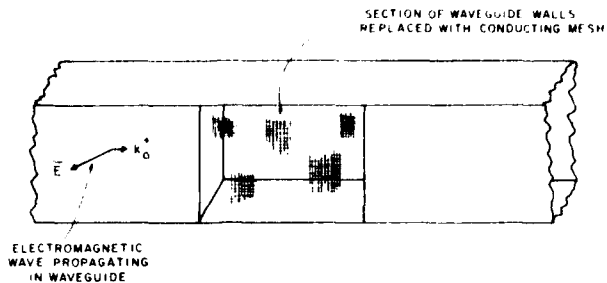


Figure 2. Waveguide walls removed and replaced with high transparency conducting mesh. Plasma inside waveguide remains physically connected to much larger surrounding plasma while interacting with electromagnetic wave

to the waveguide but allow free streaming through the waveguide of a plasma that was created throughout the experimental region. The plasma inside the waveguide was, therefore, physically connected to the much larger surrounding plasma. A pictorial diagram is shown in Figure 2.

The vacuum chamber was an aluminum cylinder, 30 cm in diameter and 45 cm long. The chamber was lined with stainless steel to insure that the plasma had a good ground connection. The combination of a roughing pump and a diffusion pump bring it to a base pressure of less than 10^{-6} Torr. Mounted on ceramic insulators inside the chamber, with insulated feedthroughs, was a framework on which more than 20 filaments, all connected in parallel, were mounted. Each filament was 10 cm long. The filaments were heated by a floatable power supply and maintained at a negative potential with respect to the chamber by another power supply. The filaments were kept at a negative 30 v. A flow-regulating leak valve was used to let argon into the system until the neutral pressure was near 10^{-4} Torr.

At each end of the chamber were circular o-ring seals for sealing on the flanges of the waveguide section which passes directly through the vacuum chamber. The vacuum chamber waveguide was 16.5 cm by 8.25 cm, a standard I.-band waveguide which mates with the other microwave components of the system. The difficult problem of creating a vacuum seal inside the waveguide was solved by using an insert of one-inch thick teflon which has a low dielectric constant and will therefore pass microwave radiation readily. Teflon also has good high vacuum properties. Careful machining of the interior of the waveguide section and the exterior of the teflon slab created a good seal between them and silicon rubber was used to form a gasket along the teflon to metal contact, which resulted in a high vacuum seal.

A 15 cm section of the waveguide walls, in the direction of the electric field, was removed from the center of the waveguide section. This was replaced with a high transparency conducting mesh. The mesh used had a transparency of 90 percent. At each end of the open waveguide sections, thin teflon sheets were placed inside the waveguide to prohibit the plasma from diffusing down the waveguide.

Ports were located on both sides of the chamber opposite the removed waveguide walls. The ports had facilities for the insertion of probes or for viewing the plasma. A leak valve, a thermocouple pressure gauge, and an ionization vacuum gauge were all located directly on the vacuum chamber. The system was water cooled with a high-flow rate for the diffusion pump and a low-flow rate refrigerated water system for the entire chamber. Figure 3 shows the relationship between the vacuum chamber, the filaments, and the waveguide sections.

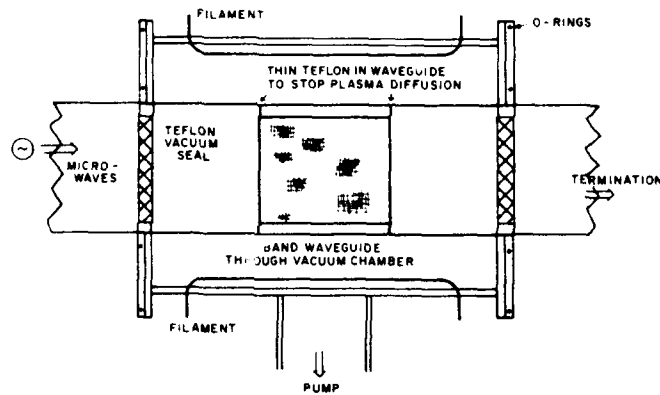


Figure 3. Vacuum chamber with penetrating waveguide. Filaments surround the waveguide and generate uniform plasma. Teflon inserts create vacuum seal at chamber walls and thin teflon inserts stop plasma diffusion down waveguide

2.1 Plasma Characteristics

The plasma density that can be maintained in an ionized gas is the result of a balance between the production and loss processes for charged particles. When the heated filaments are first biased negative relative to the wall, the entire voltage will drop uniformly between the filaments and the wall so that only a few electrons will have obtained sufficient energy to ionize an argon atom before they

strike the wall. However, once sufficient ions have been created to form a low-density plasma, this plasma surrounding the filaments will act as a cylindrical anode, a few Debye lengths from the filaments, and all electrons will enter the plasma with enough energy to ionize, as shown in Figure 4.

The plasma will lose a few of the faster electrons to the wall until its potential rises to a few electron temperatures positive and the electron and argon ion currents equalize to maintain plasma charge neutrality. With a high electron current possible, because of the small sheath at the filament and because of the slow rate of ambipolar diffusion of the plasma to the wall, the plasma will be maintained at a high density.

The plasma balance is maintained because the loss rate is determined by the density. The heavy mass of the argon ions slows the ambipolar diffusion rate. This plasma then fills the entire chamber, as shown in Figure 5.

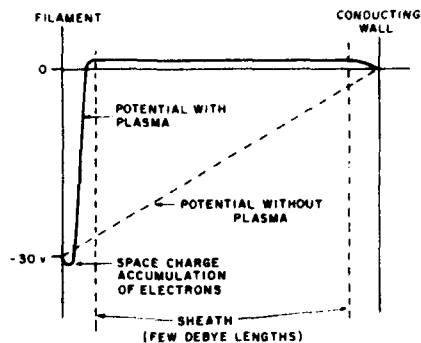


Figure 4. Plasma surrounding the filaments acts as close cylindrical anode which drops potential in a short distance and allows all electrons to enter the plasma with sufficient energy to ionize argon.

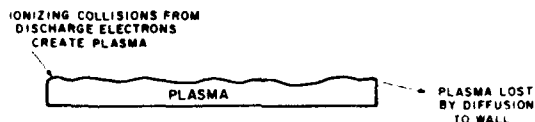


Figure 5. Plasma balance is maintained because loss rate is determined by the density. Heavy mass of argon ions slows the ambipolar diffusion rate and allows plasma to fill the chamber

Across the experimental region, inside and beyond the waveguide, the plasma density was measured and found to be uniform within a few percent.

Density fluctuations, or plasma noise, were found to be small in all regions except very near the filaments. The measured noise levels were less than

0.1 percent of the plasma density within the interaction region. The mesh between the filaments and the interaction region helped to reduce the noise level within the interaction region.

The ion temperature was relatively fixed at approximately .2 eV, which is typical for discharge plasma devices of this type.

The electron temperature, under normal operating conditions, was determined by how rapidly the electrons could relax back from the ionization process to a lower temperature. This relaxation is governed by the electron-neutral collision frequency and, therefore, by the density of neutral argon atoms. The discharge plasma device could operate at the plasma densities necessary for the experiment with neutral densities in a range from approximately 10^{-3} Torr to 10^{-4} Torr. The upper limit, 10^{-3} Torr resulted in an electron temperature of 1 eV. The lower limit, 10^{-4} Torr, had a temperature of about 3.5 eV and was limited by the large discharge currents necessary from the filaments. For these low neutral densities the filaments had very short lifetimes.

2.2 Electromagnetic Wave Source and System

The important criterion in characterizing an electromagnetic field interacting with a plasma is the ratio of the energy in the field to the thermal energy of the plasma. This ratio, η^2 , is:

$$\eta^2 = \frac{E^2}{4\pi nkT_e}$$

From the equations for the electromagnetic field in a waveguide, the magnitude of η can easily be calculated from measurements of the power being transmitted in the waveguide. These calculations were verified by RF probes in the waveguide.

The basic high-frequency signal was obtained from a microwave source operating at 1.2 GHz. The source could be pulsed, with rise times less than 100 nanoseconds. Pulsed operation stopped the generation of RF plasma.

The microwave source was protected by a ferrite isolator. Higher frequency harmonics of the basic signal, which could enter the waveguide and pass through the plasma and interfere with measurements, were filtered out with a low pass filter. This signal then went through a directional coupler where forward and reverse powers were measured with crystals. A coaxial to L band waveguide coupler transferred the signal into the waveguide sections which attached to the vacuum chamber containing the plasma. After leaving the plasma region, the signal traveled down another waveguide section where transmitted power was

measured with an RF probe. The power was finally absorbed in a very low reflection, VSWR = 1.05, waveguide load. Figure 6 shows a schematic of the experiment.

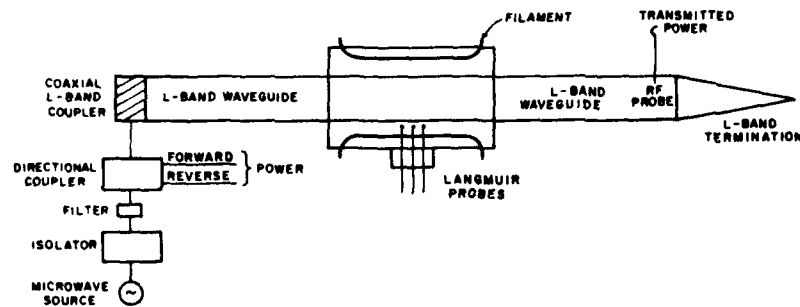


Figure 6. Experimental apparatus which allows well-defined electromagnetic wave propagating in a waveguide to interact with large surrounding plasma

The presence of standing waves in the waveguide, the result of reflections from the teflon inserts in the waveguide which formed the seals for the vacuum chamber, were found to be insignificant.

3. EXPERIMENTAL OBSERVATIONS

3.1 Threshold Conditions

The primary factor in determining, experimentally, whether or not the parametric instability was being excited, was observing that the resonance conditions were being satisfied. When the plasma density was correct for frequency matching of the driving electron plasma wave and the electron plasma frequency, high- and low-frequency spectrum analysis of probes in the plasma displayed the excitation of electromagnetic waves, electron plasma waves, and ion acoustic waves satisfying the relationship:

$$\omega_0 = \omega_e + \omega_i \quad \left\{ \begin{array}{l} \omega_0 = \text{microwave frequency} \\ \omega_e = \text{electron plasma frequency} \\ \omega_i = \text{ion acoustic frequency} \end{array} \right.$$

The energy balance equation which determined the threshold for excitation of the instability was:

$$\eta_{\text{threshold}} \approx \sqrt{\frac{V_e}{\omega_e} \frac{V_i}{\omega_i}}$$

For our normal operating conditions, the values of V_e/ω_e and V_i/ω_i , determined from both theoretical calculations and from comparison with experimental measurements under similar plasma conditions, were approximately:

$$\frac{V_e}{\omega_e} \approx 10^{-3}$$

This electron wave damping is caused by collisions, while ion wave damping results from Landau damping processes:

$$\frac{V_i}{\omega_i} \approx 10^{-2}$$

These results predict a threshold in the neighborhood of:

$$\eta_{\text{threshold}} \approx .003$$

There is some question as to the exact nature of threshold. It is often stated that the instability is excited when the first electron plasma wave is seen. However, this first wave is just a linearly unstable mode that grows up in relation to the mode damping mechanisms. Therefore, when threshold conditions are overcome, the mode would grow without limit. Because of this, threshold would probably be determined by the appearance of a second electron plasma wave, which is a definite indication of non-linear processes working.

Due to the great sensitivity of threshold conditions to variables such as small plasma density changes, electron temperature changes, and density gradients, accurate determination of thresholds was difficult. However, using the above criterion of the appearance of a second electron plasma wave, a general agreement was found with threshold being in the neighborhood $\eta = .003$.

The initial stage was the observed satellite electron plasma wave structure around the driver frequency. Up to six or more satellites were observed as the power was increased slightly above $\eta = .001$. A similar response was seen in the low-frequency ion acoustic waves. This effect is shown in Figure 7.

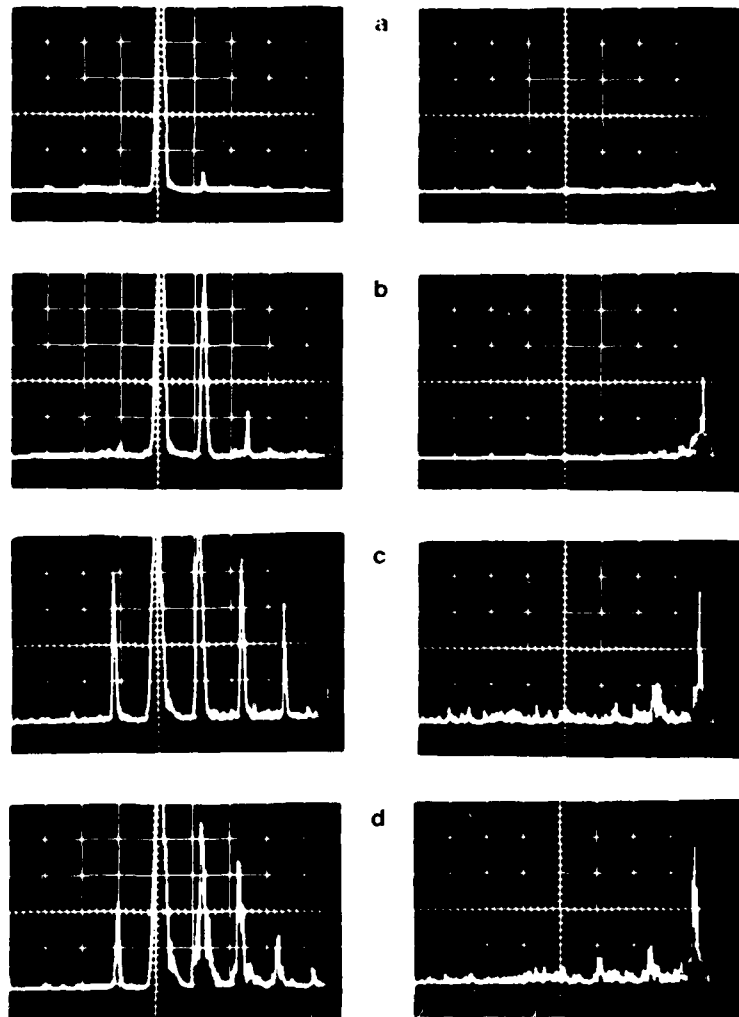


Figure 7. Threshold plasma wave spectra. Vertical scale linear in electric field. Driving electromagnetic wave frequency centered on left hatched division and 0 MHz at far right. Electron plasma waves in left frame and ion acoustic waves in right frame. One MHz per horizontal division for all frames. a) $\eta = .002$, first electron plasma wave and ion acoustic noise. b) $\eta = .004$, threshold showing two electron plasma waves growing and ion acoustic waves. c) $\eta = .007$, system of finely structured electron plasma and ion acoustic waves. d) $\eta = .008$, fine structure of electron plasma waves appears unstable and subject to frequency splitting.

In all cases it was observed that the frequency matching requirements for parametric instabilities were satisfied by the theoretically predicted electron plasma wave and ion acoustic wave:

$$\omega_0 = \omega_e + \omega_i.$$

As incident microwave power was increased and threshold passed, other electron plasma and ion acoustic waves appeared. This satellite structure of electron plasma waves suggested that each mode helped to drive the next higher mode. The coupling between these numerous modes gave rise to the intricate structure observed. The collisional damping and saturation of each individual mode would account for the overall damping and energy absorption by the plasma. The satellite structure was well-maintained to $\eta = .007$.

3.2 Breakdown of Satellite Structure

With $\eta = .008$, the satellite electron plasma wave structure appeared unstable and subject to a pronounced splitting of the finely detailed spectrum of the weak case. The individual frequencies appeared to have become overloaded and other nearby frequencies were excited. This process continued until there was a complete breakdown from the fine structure. As the electromagnetic power into the plasma was increased, the high frequencies built towards the driver frequency and then, eventually, there was more growth and a spreading away from the driver. A similar effect was seen as the ion acoustic wave spectrum built towards first lower and then higher frequencies, as if the high- and low-frequency spectrums were maintaining a kind of quasi-resonant frequency relationship.

As η increased above $\eta = .008$, background noise also increased and the individual frequencies became less distinct. By $\eta = .010$ the spectrum had reverted to a single broad frequency band at approximately the location of the original single spike. It appeared as though the original instability requirements were again being excited, only this time over a wider band of frequencies. The ion acoustic frequency spectrum exhibited a similar response. This was the first appearance of significant ion acoustic noise. Figure 8 shows the growth of turbulent plasma conditions from slightly above threshold until $\eta = .040$. Plasma waves are spread several MHz from the driving microwave frequency.

Recent computer simulations help to explain the broadbandedness of these spectrums⁵. The results show that when there is sufficient energy in the electromagnetic wave to excite plasma wave frequencies close to each other, these

5. Karan, J. (Private communication).

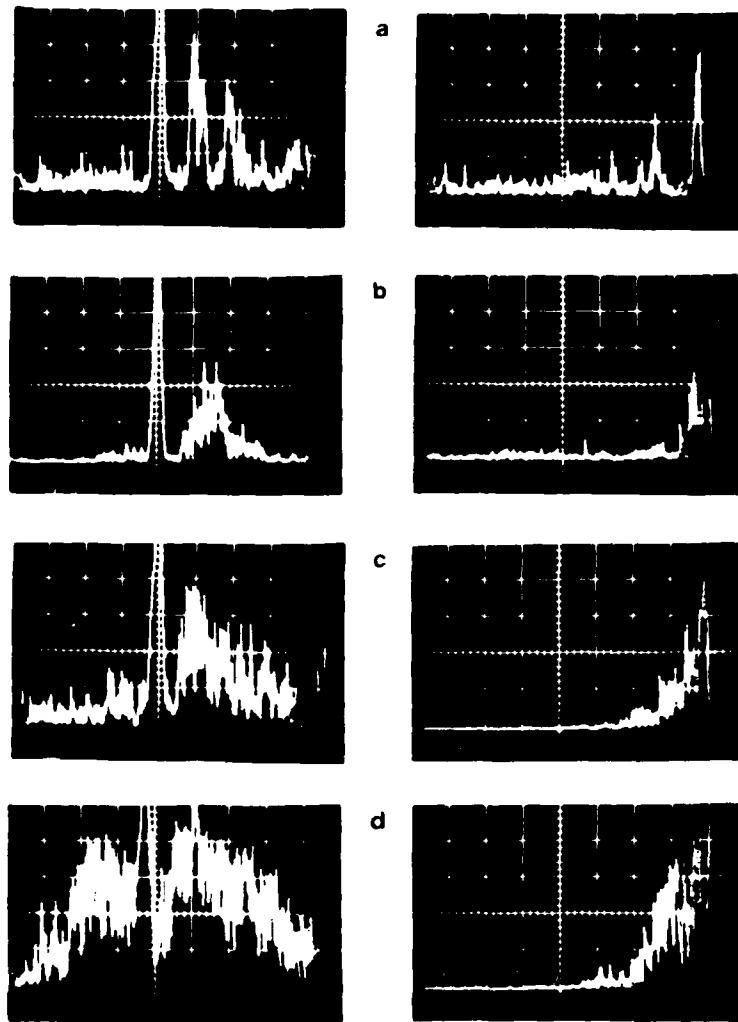


Figure 8. Plasma wave structure transition to turbulent conditions. Vertical and horizontal scales same as Fig. 7. a) $\eta = .009$, breakdown of fine structure and high level of background noise in both electron plasma wave and ion acoustic wave measurements. b) $\eta = .010$, broadband of frequencies driven near original plasma waves for both electron plasma waves and ion acoustic waves. c) $\eta = .020$, and d) $\eta = .040$, turbulent electron plasma waves and ion acoustic waves.

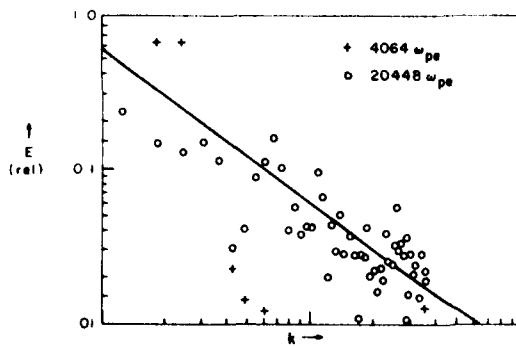


Figure 9. Computer simulation studies of electron plasma waves driven with a small frequency separation. Waves quickly couple together and energy spreads to many adjacent frequencies.

waves can quickly couple to each other and the energy will begin to rapidly spread out in frequency. This phenomena is demonstrated in Figure 9 and appears much like that observed experimentally for both the ion acoustic waves and electron plasma waves.

From $\eta = .040$ to $\eta = .070$, growth and spreading of the plasma waves was seen, but the same basic phenomena of electron plasma waves clustered about the driver was retained.

3.3 Plasma Wave Spreading to High Frequencies

As microwave power incident on the plasma was increased above $\eta = .040$, the amplitude of the electron plasma waves increased and frequencies spread away from the driving frequency in a uniform manner. When the power was approximately $\eta = .070$, plasma waves extended down in frequency to near ω_{pe} , the electron plasma frequency, and were unable to propagate in the plasma. Plasma waves then started a non-uniform frequency spread toward the higher frequencies. This frequency spread is shown in Figure 10. There is a corresponding spread in the ion plasma waves out towards the ion plasma frequency ω_{pi} .

The structure of the electron plasma wave spread toward higher frequencies is well represented by an exponential. This exponential decay is depicted in Figure 11. The exponential distribution of electron plasma waves over the broad frequency range is suggestive of a Poisson process resulting from the numerous random interactions of many plasma waves.

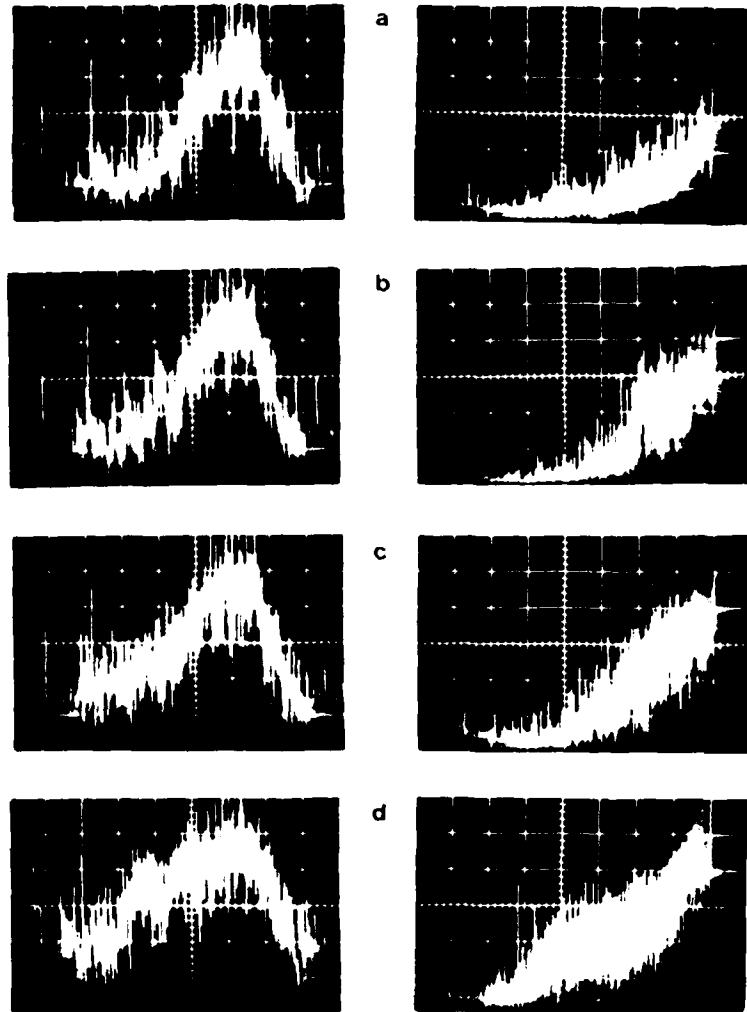


Figure 10. Turbulent plasma wave spectra. Vertical scale linear in electric field and a factor of five increase over Figures 7 and 8. Driving electromagnetic wave frequency centered one division to right of hatched division in left frames. 0 MHz is at far right. Ten MHz per division in left frames (electron plasma waves) and 1 MHz per division in right frames (ion acoustic waves). Decay of electron plasma waves assumes exponential distribution toward higher frequencies. Ion acoustic turbulence extends over several MHz. a) $\eta = .077$. b) $\eta = .084$. c) $\eta = .106$. d) $\eta = .117$.

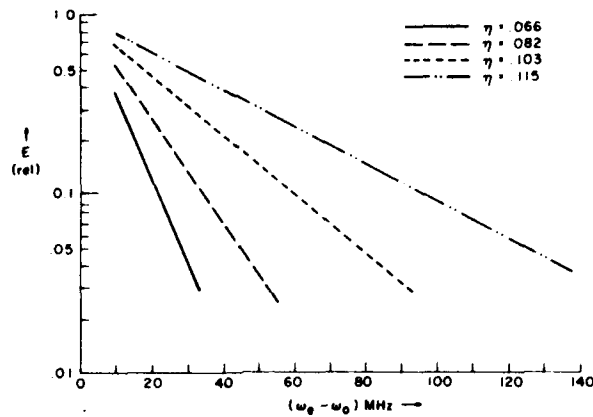


Figure 11. Electron plasma waves have exponential decay towards higher frequencies. Plasma waves stretch out hundreds of MHz at higher power levels.

3.4 Plasma Electron Heating

For η near threshold, absorption of RF power was only a small fraction of the total power incident upon the plasma. However, as power was increased above threshold, absorption increased rapidly, as shown in Figure 12. The initial part of the data, $.005 < \eta < .010$, has a slope that approximately reflects the equation:

$$P_{\text{absorbed}} \propto E^4$$

or else:

$$P_{\text{absorbed}} \propto V^* E^2$$

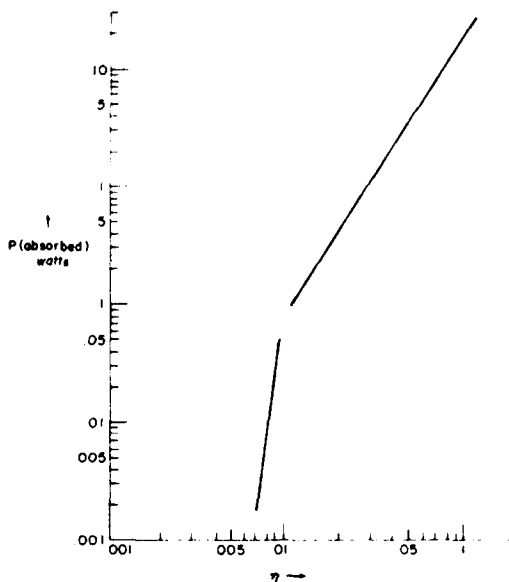
which suggests that V^* , the anomalous collision frequency, follows the relationship:

$$V^* \propto E^2$$

This result is in agreement with both theory⁶ and with other experimental data³

6. Kuren, W. L. and Valeo, E. J. (1972) Princeton PPL Matt-919.

Figure 12. Change in structure of absorbed power curve commensurate with breakdown from finely structured electron plasma waves to more turbulent plasma conditions.



for the regime near threshold. This anomalous collision frequency dependence on the electric field squared is, consequently, relevant for the discrete, finely structured *spectrum of the instability*.

For $\eta > .010$, which was approximately coincident with the start of a broad-banded spectrum and the breakdown of the fine structure, there was a radical change in the absorption pattern. By this power level, a significant fraction of the incident power was being absorbed and the rate of increase of power absorption with respect to η slowed considerably. The RF power absorbed now increased in proportion to the incident power, indicating a relatively constant anomalous collision frequency. This result is in agreement with computer simulation studies of anomalous resistivity.⁷

The electromagnetic energy which has been absorbed by the plasma must reside in the plasma particles. Plasma heating was clearly seen in an increased plasma electron temperature. Maxwellian electron energy distributions are observed in all cases for RF power less than $\eta = .1$. These distributions were clearly shown in Figure 13. The results show distributions that are Maxwellian down through more than three orders of magnitude in density.

At RF power levels above $\eta = .1$, the upper part, or lower energy region of the electron distribution, tended to stabilize with an electron temperature of

7. Kuren, W.L., et.al., (1970) Phys. Rev. Lett. 24:987.

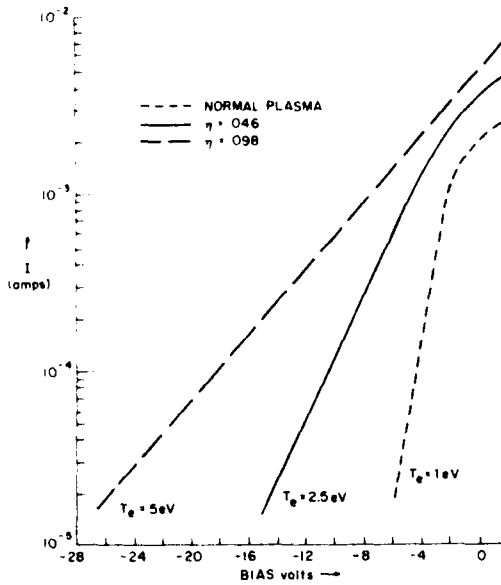


Figure 13. Electron energy distribution retains a Maxwellian energy distribution for moderate power levels.

approximately seven eV. As η was increased above $\eta = .2$, a higher temperature Maxwellian distribution was observed to break off from the seven eV distribution. This bi-Maxwellian distribution continued increasing in temperature up to the highest η used. These results are shown in Figure 14. While producing many high-energy electrons, the distribution is definitely Maxwellian in shape and therefore should probably not be considered as a high energy "tail."

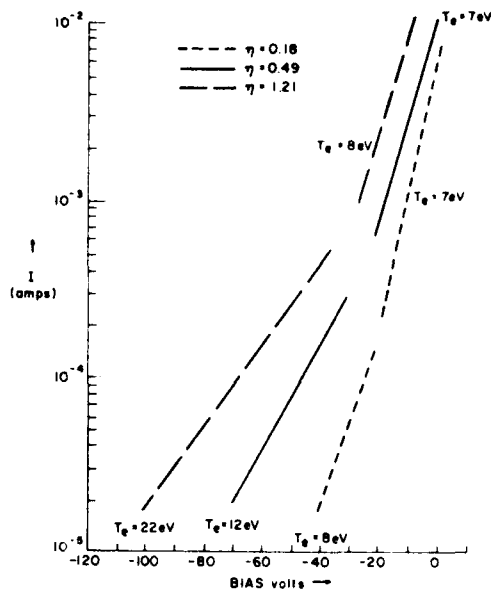
This type of bi-Maxwellian distribution can perhaps be explained by examining the strong case spectrum analysis. As η was increased up to $\eta = .2$, the frequency spectrum was stretching out hundreds of megacycles from the driving frequency. All of the electron plasma waves represented over the hundreds of megacycles of spectrum will be collisionally damped, and this collisional damping will transfer the energy to the electrons. Collisional damping will result in a Maxwellian distribution of electron energies.

As the electron plasma wave frequencies stretch higher and higher in frequency, because of their dispersion relation:

$$\omega_e^2 = \omega_{pe}^2 (1 + 3k^2 \lambda_{De}^2)$$

the higher frequencies will have greater wavenumbers, k , and the phase velocity of the waves is becoming slower and slower as k increases

Figure 14. For higher power levels the electron energy distribution splits into two segments. Lower energy portions stabilize near an electron temperature of about seven electron volts. Higher energy portions continue to increase at the highest power levels used, but retain a Maxwellian distribution in energy.



$$V_{\text{phase}} = \omega_e / k = v_{pe} (1/k^2 + 3\lambda^2 D_e)^{\frac{1}{2}}$$

When the phase velocity is sufficiently low, the electron plasma waves will be able to reach out and interact directly with some of the higher energy electrons⁸. These electrons will be accelerated as they interact with the wave.

3.5 Ion Acoustic Turbulence

Ion acoustic waves play a major role in the coupling process and were also investigated. Ion noise levels grew slowly as η was first increased, until η was near $\eta = .05$. At this point there was a rapid increase in $\delta n/n$, which continued driving the ion noise levels up to $\delta n/n$ near 20 percent. This region in the spectrum analysis corresponds to both an increase in amplitude and a tremendous frequency spreading in both the electron plasma waves and the ion acoustic waves.

The ion acoustic noise was then observed to saturate and level off with a $\delta n/n$ of around 20 percent. Spectrum analysis reveals that by this time the ion plasma waves extend out to, and sometimes beyond, the ion plasma frequency. These waves are very heavily damped by the plasma. These ion acoustic noise levels are shown in Figure 15.

8. Katz, J.I. and De Groot, T.S. (1972) UCRL-73785.

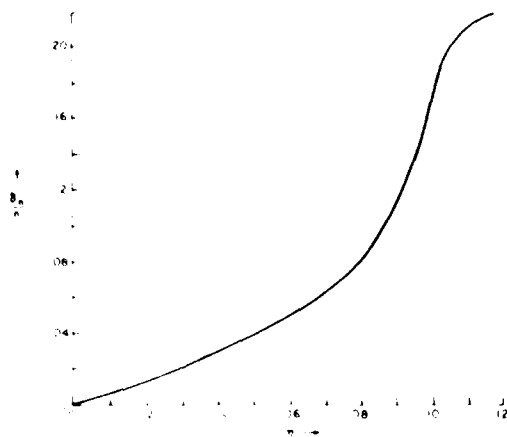


Figure 15. Ion acoustic turbulence increases to high levels and then appears to saturate at that level.

The saturation of ion turbulence may possibly be explained by ion trapping for $\delta n/n$ approaching 20 percent. Theoretical calculations⁹ for conditions approximating those in the experiment indicate this to be an important effect in limiting $\delta n/n$. For extremely high η , approaching $\eta = 1$, ion acoustic noise levels remained relatively constant.

4. SUMMARY

This experiment formed a link between the excitation of the parametric decay instability and the gross physical changes in the plasma conditions. The complete and detailed analysis of the instability spectrum has helped develop the physics behind the interaction. This physical interpretation may lead to an understanding of the great increase in the anomalous collision frequency, as demonstrated clearly in the experimental results.

The manner in which the large absorption of power changes the plasma has been shown in the result that electron energy distributions remain Maxwellian with no significant high-energy tails. The large, observed levels of ion acoustic noise are important to the coupling process, for the electrons and ions are tied together by the plasma properties. These results help bring together previous theoretical, computer simulation, and experimental investigations.

9. Dawson, J.M., Kuren, W.L. and Rosen, B. (1972) Princeton PPI. Matt-883.

References

1. Cohen, R. and Whitehead, J.D. (1970) J. Geophys. Res. 75:6439.
2. Carlson, H.E., Gordon, W.E. and Showen, R.L. (1972) J. Geophys. Res. 77:1242-1250.
3. Chu, T.K. and Hendel, H.W. (1972) Phys. Rev. Lett. 29:634.
4. Dreiser, H., Ellis, R.F. and Ingraham, T.C. (1973) Phys. Rev. Lett. 31:426.
5. Karan, J. (Private communication).
6. Kuren, W.L. and Valeo, E.J. (1972) Princeton PPL Matt-919.
7. Kuren, W.L., et al., (1970) Phys. Rev. Lett. 24:987.
8. Katz, J.I. and De Groot, T.S. (1972) UCRL-73785.
9. Dawson, J.M., Kuren, W.L. and Rosen, B. (1972) Princeton PPL Matt-883.